

# Rothamsted Repository Download

## A - Papers appearing in refereed journals

Stroppiana, D., Boschetti, M., Azar, R., Barbieri, M., Collivignarelli, F., Gatti, I., Fontanelli, G., Busetto, L. and Holecz, F. 2019. In-season early mapping of rice area and flooding dynamics from optical and SAR satellite data. *European Journal of Remote Sensing*. 52 (1), pp. 206-220.

The publisher's version can be accessed at:

- <https://dx.doi.org/10.1080/22797254.2019.1581583>

The output can be accessed at: <https://repository.rothamsted.ac.uk/item/8wy19>.

© 26 February 2019 Licensed under the Creative Commons CC BY-NC.



## In-season early mapping of rice area and flooding dynamics from optical and SAR satellite data

D. Stroppiana, Mirco Boschetti, R. Azar, M. Barbieri, F. Collivignarelli, L. Gatti, G. Fontanelli, L. Busetto & F. Holecz

To cite this article: D. Stroppiana, Mirco Boschetti, R. Azar, M. Barbieri, F. Collivignarelli, L. Gatti, G. Fontanelli, L. Busetto & F. Holecz (2019) In-season early mapping of rice area and flooding dynamics from optical and SAR satellite data, *European Journal of Remote Sensing*, 52:1, 206-220, DOI: [10.1080/22797254.2019.1581583](https://doi.org/10.1080/22797254.2019.1581583)

To link to this article: <https://doi.org/10.1080/22797254.2019.1581583>



© 2019 The Author(s). Published by Informa UK Limited, trading as Taylor & Francis Group.



Published online: 26 Feb 2019.



Submit your article to this journal [↗](#)



Article views: 299



View Crossmark data [↗](#)

## In-season early mapping of rice area and flooding dynamics from optical and SAR satellite data

D. Stroppiana <sup>a</sup>, Mirco Boschetti <sup>a</sup>, R. Azar<sup>a</sup>, M. Barbieri<sup>b</sup>, F. Collivignarelli<sup>b</sup>, L. Gatti<sup>b</sup>, G. Fontanelli <sup>c</sup>, L. Busetto <sup>a</sup> and F. Holecz<sup>b</sup>

<sup>a</sup>Istituto per il Rilevamento Elettromagnetico dell'Ambiente, Sezione Secondaria di Milano, Consiglio Nazionale delle Ricerche, Milano, Italy; <sup>b</sup>SARMAP, SA, Cascine di Barico, Purasca, Switzerland; <sup>c</sup>Rothamsted, Harpenden, UK

### ABSTRACT

Rice mapping products were derived from Sentinel-1A and Landsat-8 OLI multi-temporal imagery over Northern Italy at the early stages of the 2015 growing season. A rule-based algorithm was applied to synthetic statistical metrics (TSDs-Temporal Spectra Descriptors) computed from temporal datasets of optical spectral indices and SAR backscattering coefficient. Temporal series are available up to the tillering/full canopy cover stage which is identified as the optimum timing for delivering in-season information on rice area (i.e. mid July). The approach relies on a-priori knowledge on crop dynamics to adapt time horizons for TSD computation and thresholds to local conditions. Output products consist of maps of rice cultivated areas, rice seeding techniques (dry and flooded rice) and flooding practices. Validation showed rice mapping overall accuracy to be 87.8% with commission and omission errors of 3.5% and 24.7%, respectively. Mapping of rice seeding technique showed good agreement with farmer declarations aggregated at the municipality scale (dry rice  $r^2 = 0.71$  and flooded rice  $r^2 = 0.91$ ). Finally, flood maps have an overall accuracy above 70%. Geo-products on rice areas and flooding occurrence are relevant information for water management at regional scale especially during summer in presence of multiple crops and water shortage.

### ARTICLE HISTORY

Received 26 July 2018  
Revised 29 January 2019  
Accepted 8 February 2019

### KEYWORDS

Paddy rice; dry seeding rice; rule-based algorithm; Landsat OLI; sentinel 1

## Introduction

Early and timely information on crop type and conditions is crucial for agricultural monitoring and resource planning by private and public decision-makers (Hao, Zhan, Wang, Niu, & Shakir, 2015). In the European Union (EU), Italy accounts for more than half of the total rice production. In rice cultivations, water usage by irrigation and/or agronomic flooding is relevant although increasing use of direct dry seeding techniques can significantly change timing of water needs by rice farmers. These changes could affect water resource management and planning and lead to conflicts with other irrigated crops (Ranghetti et al., 2016). Information on rice flooding dynamics is therefore crucial for better understanding of agronomic and ecologic impacts of changes in water usage and for better planning of water provision.

Remote sensing (RS) techniques have long been exploited for land cover mapping since early 1970s with the first NASA (National Aeronautics and Space Administration) Landsat images with a specific interest in agricultural monitoring. Specifically, for rice mapping purposes, RS data proved to be valuable source of information at regional to global scales (Dong & Xiao, 2016; Fang, Wu, Liu, & Huang, 1998; Gumma et al., 2011). For

rice mapping applications, most of the literature has grown in Asia due to the relevance that rice cultivations have for food production and population survival. As reference, Asia produced 90% of the global rice in 2011 (Kuenzer & Knauer, 2013).

Data acquired by passive optical satellite sensors such as NOAA-AVHRR (National Oceanic and Atmospheric Administration-Advanced Very High Resolution Radiometer) (Fang et al., 1998), NASA MODIS (Moderate-resolution Imaging Spectroradiometer) (Shi, Huang, & Zhang, 2013; Sun, Huang, Huete, Peng, & Zhang, 2009), SPOT VEGETATION (Kamthongkiat, Honda, Turrall, Tripathi, & Wuwongse, 2005; Xiao et al., 2002), ENVISAT MERIS (MEdium Resolution Imaging Spectrometer) (Kirches et al., 2014) and Landsat TM/ETM+ (Thematic Mapper/Enhanced Thematic Mapper) (Azar et al., 2016; Yu et al., 2013) have long been used for assessing rice area extent from land cover and/or crop map products.

At regional scale, ESA (European Space Agency) Sentinel 2 and NASA Landsat satellite missions provide suitable RS data for land use/land cover mapping; despite the enhanced radiometric and geometric characteristics of the Sentinel missions, at present, Landsat data still constitute the longest archive available for

monitoring land surface (Chakraborty, Sachdeva, & Joshi, 2016). Since revisiting time might be drastically reduced by cloud cover and cloud shadows, radar RS relying on Synthetic Aperture Radar (SAR) sensors mounted on satellite platforms offers the unique advantage of not being affected by clouds and atmospheric conditions. Several studies have been carried out to investigate the potential of SAR backscatter information for rice mapping and monitoring by exploiting imagery acquired by ERS-1 (European Remote Sensing-1), RADARSAT-1 and 2, ENVISAT ASAR (Advanced Synthetic Aperture Radar) and PALSAR (Phased Array type L-band Synthetic Aperture Radar) (Bouvet & Le Toan, 2011; Cesari de Maria et al., 2016; Choudhury & Chakraborty, 2006; Oguro et al., 2001; Shao et al., 2001). However, major limitations with past satellite SAR missions were: (i) lack of systematic acquisitions, (ii) poor data availability and (iii) high cost for large-scale mapping which jeopardized the development of operational products (Bouvet & Le Toan, 2011; Dong & Xiao, 2016), until the advent of the ESA Sentinel 1 missions. Dual-polarization Sentinel-1A data are available every 12 days since the end of 2014 and the launch of Sentinel-1B (2017) increased revisiting time up to 6 days.

Multi-temporal datasets of RS images have been widely exploited for crop mapping (Brown, Kastens, Coutinho, Victoria, & Bishop, 2013). Time series of satellite images offer the opportunity to retrieve dynamic properties of target surfaces by investigating their spectral properties (both reflectance and backscatter) combined with temporal information on their changes. The availability of satellite imagery at key times during the crop growing cycle is indeed essential for more accurate discrimination. Dual-polarization SAR imagery offers enhanced capability for discriminating rice crop areas from other land cover, which were found to be characterized by very similar backscatter in single-polarization images (Mosleh, Hassan, & Chowdhury, 2015). The availability of optical and SAR data allows the scientific community to exploit advantages offered by the two technologies separately (Torbick et al., 2011). For full review of both optical and radar RS techniques applied to rice mapping and monitoring, the reader can refer to publications such as Kuenzer and Knauer (2013) and Mosleh et al. (2015).

This study was carried out in the framework of the ERMES (an Earth observation Model based RicE information Service) project (<http://www.ermes-p7space.eu/>) that aimed to develop a prototype of Copernicus downstream services assimilating EO and *in situ* data in rice crop modelling (Busetto et al., 2017). In the project's framework, rice area mapping was recognized as a major product by private and institutional users for the three study areas located in Italy, Spain and Greece. Besides being key information for

agronomic management and planning by farmers, estimating crop acreage at country scale is necessary to address EU's common agricultural policy (CAP) objectives. Moreover, rice area is one of the key input data to perform yearly based yield estimation by crop modelling (Pagani et al., 2019).

In Italy, in particular, information on rice cultivated areas are provided by Ente Nazionale Risi (ENR) on the basis of farmer declarations and distributed to users only later in the season. Moreover, this database does not possess an explicit spatial dimension and is provided aggregated at the administrative unit level (i.e. municipality). Spatially distributed information on crop cultivated areas at regional scale (i.e. regional map) was produced and delivered to the public with annual frequency by "Ente Regionale per I Servizi all'Agricoltura e alle Foreste" (ERSAF, Regione Lombardia) up to 2015. Maps were derived by processing official ENR farmer declarations and by integrating them with a land use map ("Destinazione d'Uso dei Suoli Agricoli e forestali" – DUSAF) (<http://www.ersaf.lombardia.it/>, last access January 2019). Due to the elaboration time necessary to integrate source information and to provide a reliable geo-spatial database, annual crop maps used to be released several months after the end of the summer growing season; this delay made the product of little use for real time and operational monitoring. Moreover, this operational service by ERSAF has not been funded since 2015, thus no geo-spatial information on crop areas in Italy is now regularly available.

In this work, SAR Sentinel-1A (S1A) and optical Landsat 8 Operational Land Imager (L8-OLI) multi-temporal imageries were used for early (in-season) rice mapping and monitoring over Northern Italy for the year 2015.

Three major objectives were addressed in this work: (1) to map rice cultivated areas at the early stage of the growing season, (2) to distinguish rice areas sown with direct seeding on dry soil or broadcast seeding on flooded fields and (3) to map agronomic flooding during the season. Thematic accuracy was assessed by comparison with reference data provided by field surveys, official statistics and classification of higher resolution satellite images for flooding occurrence.

## Study area

The study area is located in Northern Italy crossing Lombardy and Piedmont regions (Figure 1). Climate is continental, annual temperature range is up to 20° C between January and July and average precipitation is about 850 mm/year. The territory is an intensive agricultural region of approximately 11,250 Km<sup>2</sup>, where the most economically valuable crops are maize, rice and soybean; rice and maize are the

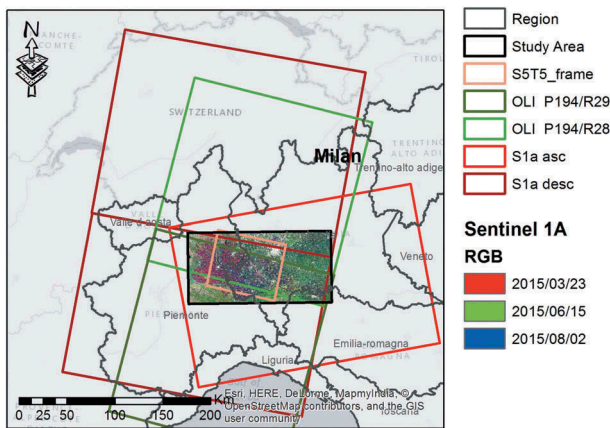


**Figure 1.** Sentinel 1A, Landsat 8 OLI and SPOT5 (Take5) frames covering the study area in Northern Italy. Background image is a false colour composite of multi-temporal S1A images (R: 23/03/2015, G: 15/06/2015, B: 02/08/2015).

most water demanding crops. Several rice varieties are cropped over about 227,300 ha (<http://www.enterisi.it>), which accounts for 90% of the total paddy rice area cultivated in Italy. Traditionally rice is cultivated in paddy fields, thus being a highly water demanding crop; but in recent years, due to water shortage and changes in timing of water availability, driven by climatic and human factors, rice cultivation techniques and systems are changing to make a more rational and sustainable use of resource (Monaco et al., 2016). Among alternative cultivation techniques is rice dry seeding, for which flooding is delayed until tillering, or rice growing as other crops with intermittent irrigation (Monaco et al., 2016; Ranghetti et al., 2016). According to recent figures (ENR, 2016), water seeding rice cultivated area has decreased of about 38% in favour of dry seeding (+53%) reaching more than 50,000 ha in 2015 (Monaco et al., 2016). Ranghetti et al. (2018) investigated the variation in irrigation dynamics over the last 17 years in the study area.

## Data and pre-processing

### Remotely sensed data

The RS dataset is composed of both optical (L8-OLI and SPOT 5) and SAR (S1A) images over the study area as shown in Figure 1. The L8-OLI multi-temporal dataset is composed of 13 scenes, from 30 September 2014 to 4 June 2015, over frames 194/029 and 194/028 (path/row). Images in the autumn/winter season were selected to mask out winter crops and enhance the accuracy of rice mapping. Rice is traditionally cultivated as summer crop with no preceding crop, with the exception of fields where cover crop practice is adopted. The use of cover crops rather than leaving bare fields during autumn/winter is a mean for ecological intensification of arable systems and for enhancing productivity by

reducing the impact of anthropogenic inputs (Wittwer, Dorn, Jossi, & van der Heijden, 2017).

L8-OLI Surface Reflectance High Level Data Products images were downloaded from the USGS Earth Resources Observation and Science (EROS) Center Science Processing Architecture (ESPA) On Demand Interface (<https://espa.cr.usgs.gov>, last access January 2019) together with the Enhanced Vegetation Index (EVI) (Huete et al., 2002) (Equation 1). Red (band 4) and short wave infrared (SWIR, band 7) reflectance bands at 30 m spatial resolution were used to compute the Normalized Difference Flooding Index (NDFI) (Equation 2) to distinguish standing water from soil and vegetation (Boschetti, Nutini, Manfron, Brivio, & Nelson, 2014). The L8-OLI dataset was re-projected to ETRS89 LAEA (Europe Lambert Azimuthal Equal Area).

$$EVI = 2 \frac{\rho_{NIR(b5L8OLI)} - \rho_{RED(b4L8OLI)}}{\rho_{NIR(b8OLI)} + 6\rho_{RED(b4L8OLI)} - 7.5\rho_{BLUE(b2L8OLI)}} \quad (1)$$

$$NDFI = \frac{\rho_{RED(b4L8OLI)} - \rho_{SWIR(b7L8OLI)}}{\rho_{RED(b4L8OLI)} + \rho_{SWIR(b7L8OLI)}} \quad (2)$$

The S1A dataset is composed of 17 C-band dual-polarization VV/VH scenes between 23 March and 1 July 2015. Image product is Ground Range Detected (GRD) Level 1 (L1), acquired in Interferometric Wide Swath (IW) mode. Since the S1A sensor acquires on the study area with a very similar incidence angle ( $\sim 35^\circ$ ) for the ascending and descending passages, both configurations were used, to enhance frequency of observation up to 4 and 8 days from ascending and descending pass, respectively. SAR images were pre-processed with Sarmap MAPScape-RICE software following the steps: (i) filtering with De Grandi multitemporal speckle filter (De Grandi, Leysen, Lee, & Schuler, 1997), (ii) geocoding to ETRS89 LAEA and (iii) radiometric calibration to Sigma Nought ( $\sigma^0$ ) by using elevation data from the Shuttle Radar Topography Mission (SRTM) 90 m Digital Elevation Database v4.1 (SRTM DEM). After pre-processing, S1A imagery is provided at 30 m spatial resolution comparable with L8-OLI indices.

The satellite dataset is completed with images acquired within the SPOT5 (Take5) (S5T5) experiment jointly conducted by CNES (Centre National d'Etudes Spatiales) and ESA to deliver simulated image time series of ESA's Sentinel-2 data (<https://spot-take5.org/client/#/home>, last access January 2019). The S5T5 dataset is composed of 25 images available from the High Geometric Resolution 2 (HRG2) instrument on board the SPOT5 platform and delivered as Level2A products (Top Of Atmosphere Reflectance) with 4 bands in the visible, near-infrared and shortwave infrared wavelengths and a spatial resolution of 10 m. The

area covered by the S5T5 dataset is highlighted by the red rectangle in Figure 1. Images covered the period 24 April to 9 September 2015. Cloud and cloud shadows were removed and NDFI (Equation 2) was computed from red and SWIR bands and used to produce reference flooding maps. Since S5T5 images cover only a portion of the study area, they were used as an external independent reference dataset to validate flooding mapping results.

### Ancillary and in situ data

Land cover information was derived by mosaicking the 2014 Lombardy land cover map (<http://www.ersaf.lombardia.it>) and the 2008 Land Cover Piemonte (<http://www.regione.piemonte.it>) at 30 m resolution and projected to ETRS89 LAEA. Pixels belonging to urban, anthropic, forest, shrub and other minor classes have been aggregated to produce a non-agriculture land cover mask. This mask was combined with altitude and slope information, computed from the SRTM DEM (Shuttle Radar Topography Mission Digital Elevation Database v4.1), to derive a mask of arable/non-arable (AL) lands.

During the 2015 growing season (April–September), *in situ* observations on crop type, crop phenology and conditions were collected with a smart application (Bordogna et al., 2016) during extensive field campaigns over the study area. In the early season, different regions of the study area were surveyed in order to characterize rice conditions and rice management over the entire study site. In the Smart-App, geo-referenced observations, collected by pinpointing the field under observation, are automatically assigned to field cadastral polygons. The smart application stores semi-structured geo-referenced *in situ* observations collected by field operators and/or farmers to support processing and interpretation of Earth Observation (EO) data for agricultural monitoring. Moreover, it offers functionalities for uploading information on crop conditions such as free text, photographs, crop type and phenology and agronomic practices, which are observed in the field and/or provided by the farmers. This ancillary information collected by the field operator could be further exploited for data interpretation. Polygons were reviewed in order to represent the actual *in situ* conditions (Villa, Stroppiana, Fontanelli, Azar, & Brivio, 2015) leading to a reference polygon layer composed of *rice* (542) and *no rice* (676) classes. The *no rice* class covers different crop types: cereals, forages, maize and soybean. This dataset was used for accuracy assessment of the rice map.

In addition to field surveys, ENR provided statistics, on rice cultivated area, varieties and yield, and rice seeding technique (water or dry seeding), which were used to assess the accuracy of dry and flooded

seeded rice mapping. These statistics, derived from farmer declarations, are aggregated at the municipality scale; a total of 277 municipalities were part of the dataset over the study area. The range of municipality surface is 172.2–18,166.34 ha with median values of about 1433 ha.

### Methods

The flowchart of the processing steps for both optical and SAR data is depicted in Figure 2 where the steps for rice mapping are highlighted by the red rectangle (“*Rice mapping module*”). The input features to the rule-based algorithm and threshold values are summarized in Tables 1 and 2.

#### Early rice mapping: temporal spectral descriptors approach

In order to produce early season rice map, we applied a pixel-level rule-based approach relying on features derived from the temporal profiles of SAR backscattering coefficient and optical spectral indices. The within-season temporal dynamics of the signal measured by EO sensors are strictly related to physiological changes during crop growing; the extraction of key parameters from the temporal profile built from multi-temporal datasets of satellite imagery is a widely used approach for crop mapping and classification (Ghazaryan et al., 2018). These approaches rely on the use of spectral metrics related to phenology (e.g. flowering period) and/or management (e.g. changes from bare soil to vegetation cover) for building classification rules based on crop calendar and phase-dependent crop conditions (Zhong, Hu, Gong, & Biging, 2016 and references herein).

In these approaches, “local” a-priori knowledge on rice calendar, crop practices and agro-ecological conditions are necessary to perform accurate mapping (Campos-Taberner et al., 2017). However, in our case study, the challenge was to define diagnostic features to map rice at the early stages (from bare soil conditions to tillering/full canopy phase), thus “looking” at a temporal window rather than the whole profile depicting the entire rice growing cycle. Moreover, the Italian rice district is a particularly complex agricultural system with more than 100 varieties belonging to both *Indica* and *Japonica* groups with either a medium (120–130 days; e.g. Gladio, Thaibonet, Selenio, Loto, etc.) or long growing cycle (>150 days; e.g. Carnaroli, Volano, Baldo, etc.) (for more details see Boschetti, Stroppiana, Brivio, & Bocchi, 2009). In recent years, the diffusion of dry seeding added further complexity in RS rice detection usually based on the identification of flooding (Boschetti et al., 2017; Nelson et al., 2014).

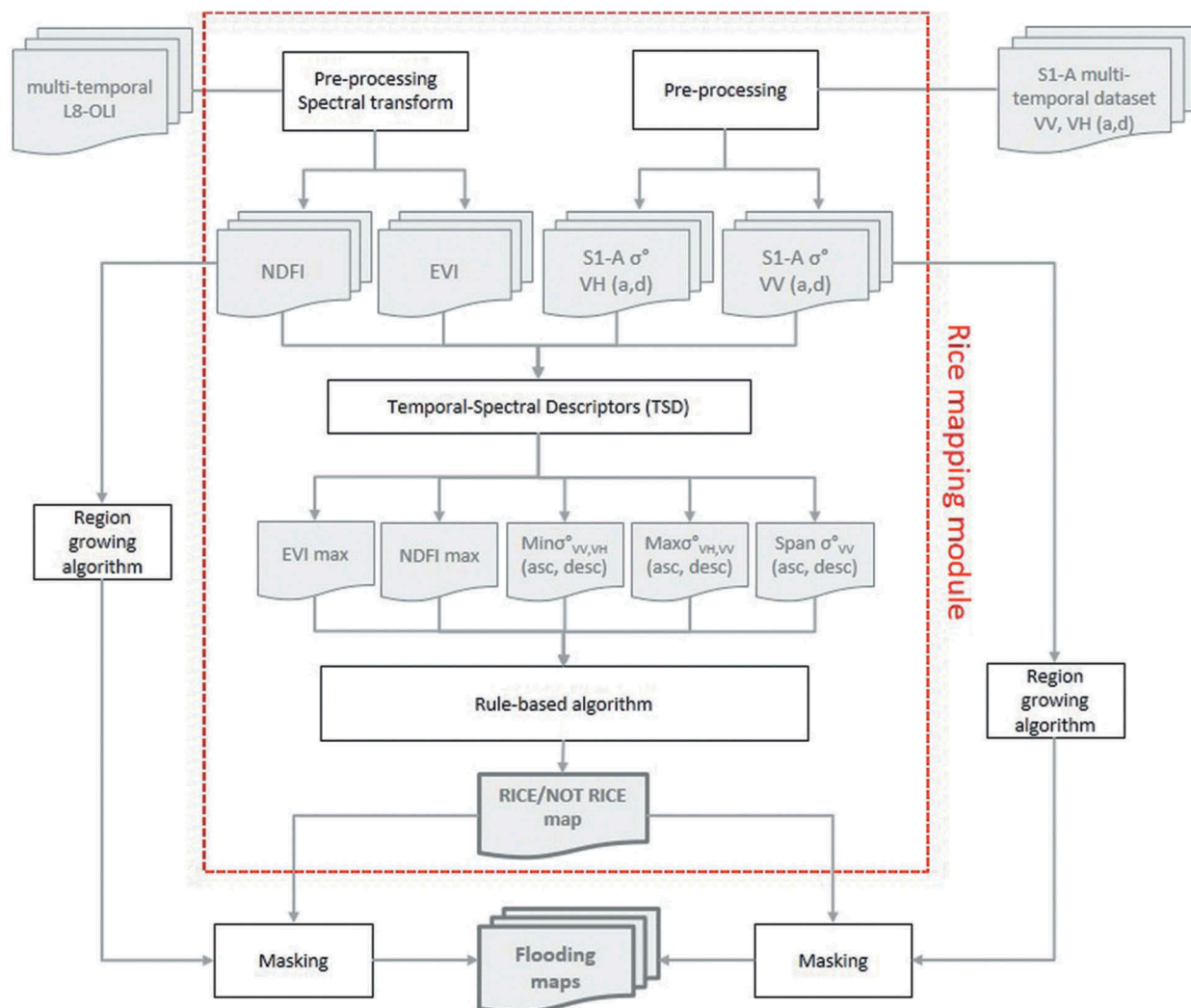


**Figure 2.** The flowchart of the algorithm implemented to produce the rice/not rice and flooding maps. The “Rice mapping module” (red rectangle) highlights the steps for producing the rice map. A region-growing algorithm is applied to derive flooding maps.

**Table 1.** Temporal Spectral Descriptor (TSD); subscripts a and d stand for ascending or descending.

TSD	Metric in relation to crop condition	Description
Min $\sigma_{VVa/d}^0$	Minimum value in the land preparation period <sup>1a</sup>	Flood status of paddy rice fields – unique feature for rice cultivation detection
Max NDFI	Maximum value in land preparation period <sup>1b</sup>	
Max $\sigma_{VHa/d}^0$	Maximum value at the end of stem elongation phase <sup>2</sup>	High biomass of summer crops – typical of summer crops
Span $\sigma_{VVa/d}^0$	Maximum-Minimum difference from tillering to stem elongation phase <sup>3</sup>	Rapid crop growth after flooding – typical of rice
Max EVI	Maximum value in the autumn/winter vegetative phase <sup>4</sup>	Winter crop presence – typical of double crops; this agro practice is not usual in temperate European rice

**Typical calendar period in the study area**

- <sup>1a</sup>March/July;  
<sup>1b</sup>April/June;  
<sup>2</sup>May–June;  
<sup>3</sup>March–July;  
<sup>4</sup>September–May.

**Table 2.** The rule-based algorithm for dry and flooded rice.

Rule	Dry rice	Flooded rice	Description
1	Max EVI < 0.3 AND (Max $\sigma_{VHa}^0$ OR Max $\sigma_{VHa/d}^0$ ) < -16 dB	Max EVI < 0.3 AND (Max $\sigma_{VHa}^0$ OR Max $\sigma_{VHa/d}^0$ ) < -15 dB	Biomass low at both early stages and later being rice less productive crop
2	Max NDFI > 0.3 AND (Min $\sigma_{VVa}^0$ OR Min $\sigma_{VVd}^0$ ) < -12.5 dB	Max NDFI > 0.3 AND (Min $\sigma_{VVa}^0$ OR Min $\sigma_{VVd}^0$ ) < -15.5 dB	Identification of rice flooding and/or field levelling
3	(Span $\sigma_{VVa}^0$ OR Span $\sigma_{VVd}^0$ ) > 4.0 dB	(Span $\sigma_{VVa}^0$ OR Span $\sigma_{VVd}^0$ ) > 4.0 dB	Rapid rice growth

The selected features input to the rule-based algorithm is synthetic statistical metrics (Temporal-Spectral Descriptors, TSD) derived from the temporal profiles of S1A backscattering coefficients  $\sigma_{VV}^0$  and  $\sigma_{VH}^0$  and L8-OLI spectral indices EVI and NDFI. TSD are defined over temporal windows related to the agro practices (e.g. land preparation and agronomic flooding) and/or to early phenological stages of rice to make the algorithm flexible enough to be adapted to different conditions with expert knowledge on rice calendar (Table 1). TSD are related to both crop growing features and field conditions at the beginning of the rice season and during the preceding winter season (i.e. relying on the fact that rice in the study area is traditionally grown as single crop cycle).

Since S1A ascending and descending orbits have different flight directions with respect to the North, the same surface area is viewed with different geometries; thus, the two temporal series were processed separately to extract both co-polarized (VV) and cross-polarized (VH) backscattering. The following TSD were computed: minimum, maximum and difference between maximum and minimum values (i.e. span), which are indicators of the presence of flooded conditions, rice biomass accumulation and rapid rice growth after flooding, respectively. As we specified above, TSD are computed over different time horizons to be diagnostic indicators of rice growing and/or agronomic practices for the discrimination between rice and other crops (Asilo et al., 2014; Fontanelli et al., 2014; Villa et al., 2015) (Table 1). Both time horizons and the threshold values can be adapted and refined to different crop and environmental conditions.

MaxEVI is an indicator of biomass accumulation suitable for discriminating presence/absence of vegetation (i.e. crop); it is computed over the September–May period when no other crop is traditionally cultivated if rice is foreseen for the following summer season. On the contrary, as knowledge on agro-practices of the study area suggests, high MaxEVI during winter identifies fields where winter cereals or forages are traditionally cultivated; indeed, these crops are not combined with rice in a double crop cycle.

In the recent years, this tendency has been slowly changing with the introduction, for example, of cover crops during the winter season preceding rice cultivation. If the use of winter cover crops in rice fields spreads in the future, this TSD could be modified by distinguishing between cover crops and winter cereals or forages, which have greater biomass in spring (e.g. higher EVI) and are harvested later in the season (i.e. beginning of June), i.e. after rice seeding (April).

MaxNDFI and SAR co-polarized minimum value of the backscattering coefficient (Min  $\sigma_{VVa/d}^0$ ) are complementary indicators of flooding, which is traditional practice for rice cultivation in Italy. Extremely

low value of SAR backscatter coefficient could also characterized laser-levelled bare fields (i.e. very low surface roughness) where specular-like backscattering effect occurs; these conditions are also typical of rice field preparation when dry seeding technique is used, thus reinforcing the role of this feature in the algorithm. SAR TSD maximum cross-polarized backscattering coefficient (Max  $\sigma_{VHa/d}^0$ ) and difference between maximum and minimum values of co-polarized backscattering (Span  $\sigma_{VVa/d}^0$ ) over the spring/summer period are, respectively, indicators of rice biomass accumulation and rapid rice growth after flooding. Clearly, this last condition is meaningful only if used in combination with the preceding ones, which identify the absence of high biomass (i.e. winter crops) and the presence of flooding/laser-levelled field conditions.

In the rule-based algorithm, a pixel is labelled as *rice* if it is not covered by vegetation in winter (Rule 1), it is levelled and/or flooded at the beginning of the season (Rule 2) and it is rapidly covered by vegetation (Rule 3). Threshold values were defined with an expert-based trial and repeat approach to identify *dry* and *flooded* seeding rice classes (Table 2). The rule-based algorithm was applied to all arable land pixels in the AL mask.

### Flooding mapping: region-growing algorithm

S1A  $\sigma_{VV}^0$  multi-temporal images were exploited to generate flooding maps. Previous studies (Twele, Cao, Plank, & Martinis, 2016) comparing the two standard polarizations, VV/VH, showed that for flooding mapping purposes, VV performed better, hence only S1A backscattering images in VV configuration were exploited. Since rice flooding is a very dynamic phenomenon related to agronomic practices, each satellite acquisition was processed separately to identify the presence or absence of water. This way, the frequency of observation is maximized and flooding dynamics (presence, start and end dates) can be monitored.

A region-growing (RG) algorithm was applied to identify rice pixels where the surface is covered by water. Seed pixels were identified by applying a conservative threshold ( $\sigma_{VV}^0 < -14.5$  dB) and grown over neighbouring pixels with stopping criterion of  $\pm 2$  standard deviations; the output is a binary *flooded/not flooded* map. The RG algorithm allows the identification of flooding conditions from highly probable flooded pixels by connecting neighbouring pixels with lower probability; this approach helps in balancing commission and omission errors by exploiting the spatial correlation (Bastarrika et al., 2011; Stroppiana et al., 2012). The algorithm was implemented in ITT HARRIS IDL®.

### Accuracy assessment

The accuracy of the early rice map was assessed by comparison with *in situ* observations collected during the 2015 rice growing season (see section Ancillary and *in situ* data). Reference polygons were labelled as *rice* and *no rice* with a majority criterion over the full resolution rice map; hence, the error/confusion matrix shows the number of polygon for agreement/disagreement. Accuracy metrics (Overall Accuracy, OA; Kappa coefficient, Kappa; Commission and Omission Errors, CE, OE) were then computed. Since *in situ* observations do not provide detailed information for *dry* and *flooded rice*, accuracy assessment was performed for the rice class as a whole.

Evaluation of the *dry* and *flooded rice* classes was done by correlation analysis between estimated surfaces and ENR statistics available at municipality scale. For each municipality belonging to the study area, EO-derived rice area estimates were compared

to ENR statistics for the *dry*, *flooded* and *total rice* classes. The error was analysed as a function of the size of the municipalities, which were aggregated into three categories (hereafter named c1, c2 and c3) based on break values computed from minimum, maximum and 33% and 66% quantiles ( $q_1 = 1091.8$  ha,  $q_2 = 1820.5$  ha). Both absolute and per cent error were analysed, i.e.  $100 * (\text{total area ENR} - \text{total area EO}) / (\text{total area ENR})$ .

Flooding maps derived with the RG algorithm were compared to reference maps derived by applying an image-based threshold to S5T5 NDFI. Visual refinement of S5T5 flooding maps was carried out by photo-interpretation of RGB false colour composites (R: SWIR, G: NIR, B: red) to obtain the most accurate reference maps for the three dates of simultaneous acquisitions with S1A images (5 May, 22 May, 1 July). [Figure 3](#) depicts example images and maps of the flooding reference dataset derived from S5T5 imagery. Over the area covered by the S5T5 frame, pixel-by-pixel

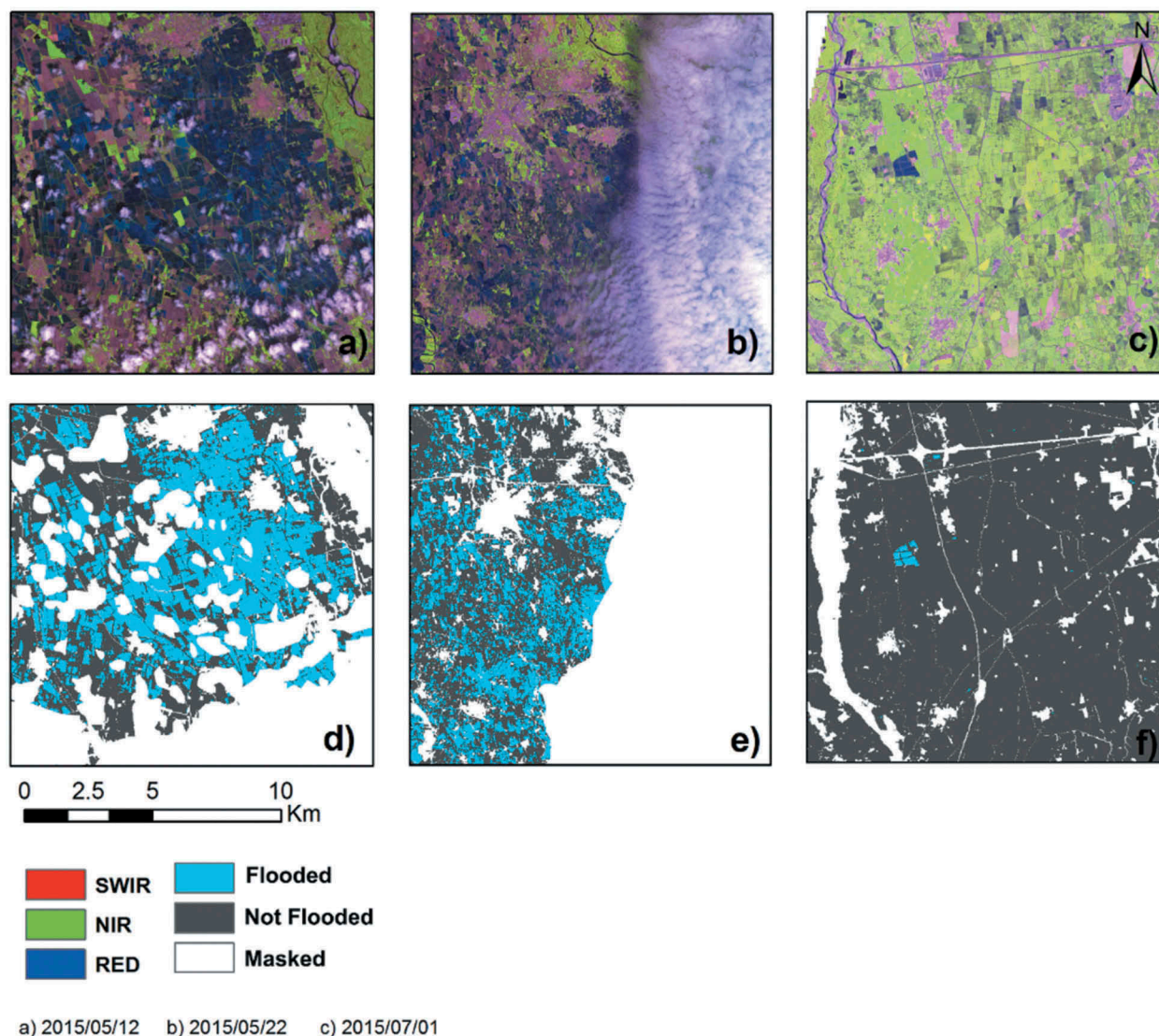


**Figure 3.** False colour composite (RGB: SWIR, NIR, red) of S5T5 images acquired on 12/05 (a), 22/05 (b) and 01/07 (c) and the reference flooding maps derived by photo-interpretation for the same dates (light blue is flooded, dark grey is not flooded, white is masked). Images are shown over zoom areas in the study area.



with intra-class variability. Finally, the maximum cross-polarized backscattering coefficient for rice is lower than other crops ( $***p < 0.001$ ) probably due to the lower biomass amount. No significant difference was observed between TSD from ascending and descending acquisitions with the only exception of  $\min \sigma_{VH}^0$ . As for the minimum co-polarized backscatter, two threshold values were employed for the rice classes. The selected TSD are exploited in conjunction in the rule-based algorithm hence, no single feature is expected to provide the highest power for separating rice from the other crops.

### Early rice and flooding mapping

Figure 5(a) shows the early rice map (mid-July) with *dry* (yellow) and *flooded seeding rice* (orange) covering 112,300 ha and 64,570 ha, respectively: *flooded rice* prevails in Piedmont (western part, orange) and *dry rice* in Lombardy (eastern part, yellow). Figure 5(b) shows the frequency of flooding computed with respect to the total number of satellite images available over the study period (i.e. 24).

Validation showed that out of 1218 fields (i.e. polygons) surveyed in 2015, 408 and 661 were correctly identified as *rice* and *no rice*, respectively, leading to OA = 87.8%, Kappa = 0.75, rice CE = 3.5% and rice OE = 24.7%.

Within the framework of the FP7 ERMES project, the algorithm proposed in this work was further applied to L8-OLI and S1A time series in 2016 over the same study area. The output product was validated with *in situ* observations collected with a smart application achieving OA = 88.2% and kappa = 0.76 (number of *in situ* point observations over the study area ~3200) and confirming the validity of the proposed approach. The 2016 rice map and validation points together with the

confusion matrix are provided in Supplementary materials (S1). An example of the spatial agreement of RG flooding maps and S5T5 reference flooding maps for the simultaneous dates of acquisition is depicted in Figure 6; in the first column, orange and blue regions show correctly classified *not flooded* and *flooded* pixels, respectively. In the figure non arable lands are grey whereas cloudy pixels are white highlighting the limitation imposed by optical satellite imagery and strengthening the contribution of SAR data for operational monitoring. In the same figure, the accuracy of the flooding maps is compared to grey scale L8 NDFI (second column) and reference flooding maps derived by applying a threshold to L8 NDFI.

Pixel-by-pixel comparison provided OA across the three dates of 88.5%, 70.2% and 99.4%. The highest OA values are achieved at end of July when no flooding is detected due to full canopy condition. Furthermore, at later stages of the growing season, both radar backscattering (S1A) and optical reflectance (S5T5) coefficients are influenced by the presence of rice plants rather than water on the background, thus preventing the detection of flooding. Yet, information on flood are necessary for water management mainly at the early stages of the rice growth cycle, because they can also be diagnostic of adopted sowing technique.

### Comparison with official data

Figure 7 shows scatter plots between total, *flooded* and *dry rice* area estimates and official ENR statistics in each municipality of the study area as well as the total rice per cent error [%] as a function of the actual total rice area (ENR). In all panels, each point represents a municipality with filling colour given by its

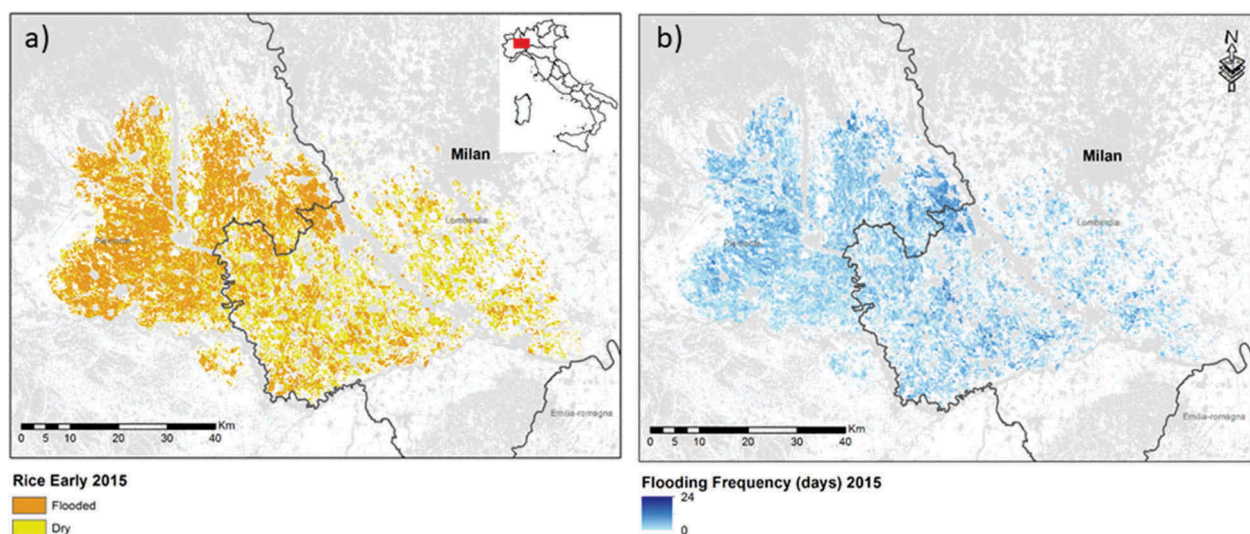
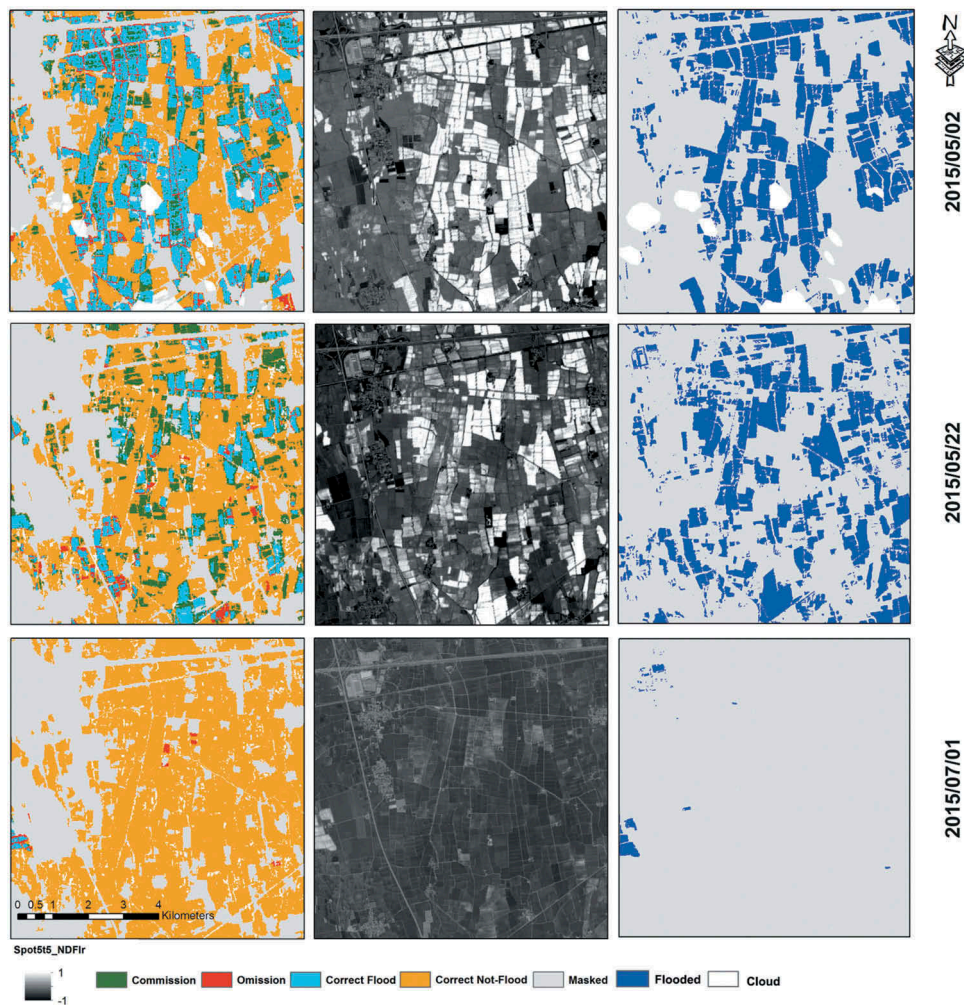


Figure 5. Early maps of (a) *dry* and *flooded* seeding rice area and (b) flooding frequency over the study period. Grey regions are non-arable lands and dark grey line shows the administrative border between regions.



**Figure 6.** Spatial distribution of the accuracy of flooding maps over three example areas for the dates of simultaneous acquisitions: accuracy map (left), L8 NDFI (middle), reference flooding map (right).

size, as reclassified into three classes based on the histogram: smaller (larger) municipalities are blue (yellow) and intermediate size is green.

Scatter plots show more than satisfactory agreement with  $r^2$  of 0.91, 0.91 and 0.71 and Mean Average Error (MAE) of 179.2, 129.2 and 142.5 ha for total, flooded and dry rice estimates, respectively. The greatest agreement occurs for flooded rice due to the presence of water before and during sowing that is univocally detected by both optical and SAR TSD. Even though dry rice detection is more challenging, the rule-based algorithm performs significantly well-being able to represent the variability of agro-practices in the different municipalities.

The distribution of the scatter points along the domain of the x-axis (actual total rice area, ENR) confirms that larger municipalities not necessarily have larger rice cultivated areas since the agricultural landscape can be fragmented (i.e. different crops in the same area). In the graph (Figure 7(d)), the y-axis range was set to  $[-100\%, 100\%]$ ; all points fall within this interval except for 10 municipalities where errors are above 100%. Among them, eight have total rice area below 25 ha, hence representing small and sparse fields

covered with very few pixels potentially in mixture condition. None of the municipalities have errors below  $-100\%$ . Generally, EO approach underestimates rice area and bias (actual-predicted) is positive: fewer points fall below the red line in Figure 7(d).

Figure 8 depicts some statistics on the rice area and errors of EO estimations aggregated over municipality area; the size category of each municipality is shown in panel a. The distribution of the errors is shown in panels b, d, f and actual total rice area and the proportion of flooded rice in panels c, d. These maps show that absolute errors are uniformly distributed over the study area (mean = 121.2 ha, median = 62.2 ha).

## Discussion

The rule-based algorithm relies on the multi-temporal trend of both SAR and optical features (VIs and backscattering coefficient) which are summarized by synthetic statistical metrics such as minimum and maximum values (TSD). Knowledge of both crop characteristics and agro-practices are exploited to set rules able to discriminate rice among other crops. Rice is traditionally cultivated as single crop and in

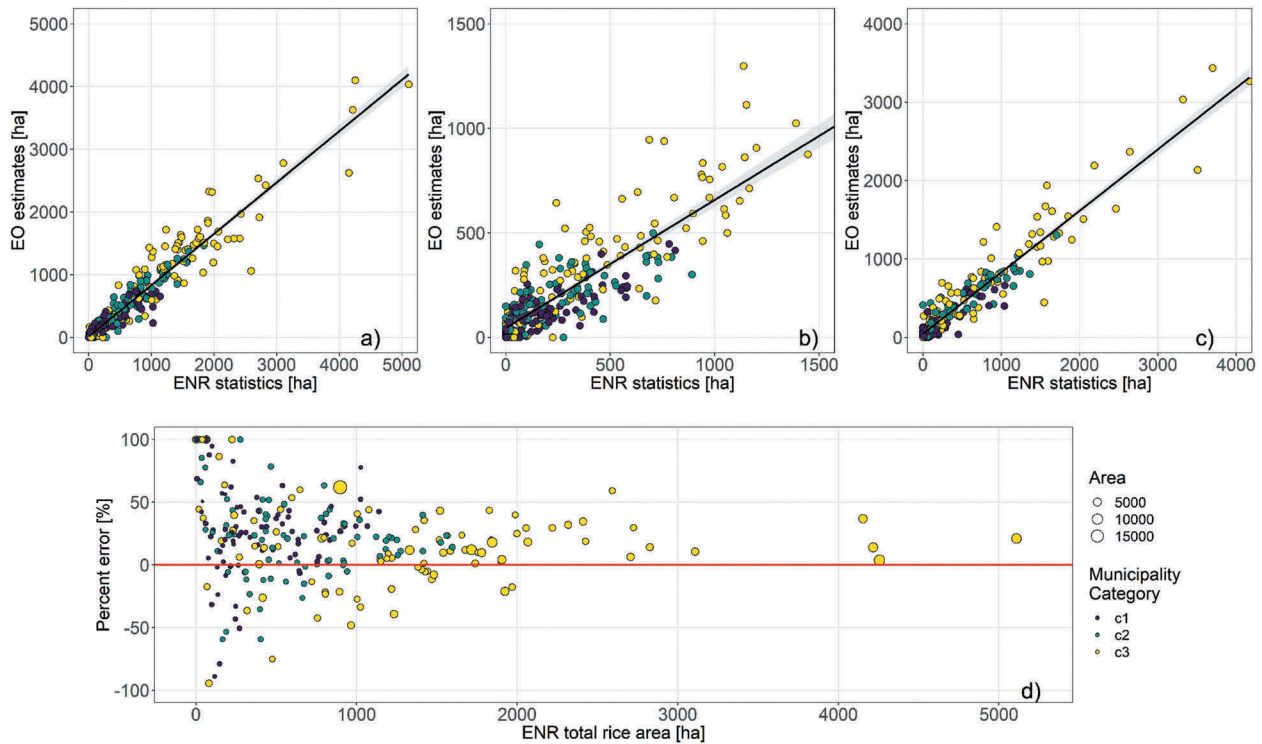


**Figure 7.** Scatter plots of EO estimated (y-axis) and ENR statistics (x-axis) of total (a), *dry* (b) and *flooded rice* (c) area [ha] for each municipality shown by the coloured circle markers; colour is the size category. In the bottom row, the per cent error ( $100 * (\text{total area ENR} - \text{total area EO}) / (\text{total area ENR})$ ) as a function of the ENR total rice area for each municipality; each marker is proportional to the size of the municipality and the colour represents the size category.

paddy fields; this unique condition is depicted by the MaxEVI feature which allowed us to discard fields where summer crop is preceded by winter cultivations. The spectral signal induced by the presence of water over the field is identified in the most sensitive SAR and optical features: NDFI and  $\sigma_{VV}^0$ , as confirmed by the analysis carried out over field observations (Figure 4 and Table 3).

The use of pheno-spectral metrics, which are derived from a temporal profile depicting crop growing, in classification algorithms has been widely exploited in the literature; however, in our specific case study the challenge was to define features based on the availability of spectral data only from the early stages of the rice growing cycle. In fact, we exploiting changes in the time-spectral domain related to agro-practices and phenological stages in order to deliver in-season information for crop management and crop planning. TSD are, indeed, defined based on the early rice phenological stages which, in the study area, assume values proposed in Table 1; however, values could be flexibly tuned over different rice cropping systems and calendars.

The proposed TSD and the rule-based algorithm can be exported and applied to different years and/or regions as long as the necessary a-priori knowledge on crop characteristics, agro-practices and environmental conditions are known. Expert knowledge is necessary to tune time horizons and thresholds to specific conditions. It is not within the scope of our

work to provide a generally valid algorithm to be applied in an automated and unsupervised way elsewhere. Yet, the algorithm as proposed here could be exploited as initial setting for trial and error for tuning to specific conditions.

The combination of rules in the decision tree-like algorithm produces a rice map with OA = 87.8%, Kappa = 0.75, rice CE = 3.5% and rice OE = 24.7%, which is more than acceptable being an early season detection. As a term of comparison, Vaudour, Noiro-Cosson and Membrive (2015) achieved a per-field OA of 69% for early-season mapping of crops in France. The greater value of the omission error might be due to the small size of rice fields; the enhanced spatial resolution of ESA Sentinel 2 data, replacing and/or complementing Landsat data for recent years could improve the accuracy of detection of small fields. Another source of omission could be the revisiting time of 4/8 days for S1A (obtained by combining ascending and descending acquisitions) and 16 days for L8-OLI that might lead to a lack of observations at key stages of rice sowing, flooding and growing; although only these RS datasets were available when the work was carried out, the present availability of S1B and Sentinel 2 (A&B) data will mitigate this effect for future applications (Nguyen, Gruber, & Wagner, 2016).

The algorithm was further applied to the 2016 rice season achieving comparable accuracy levels (OA = 88.2% and kappa = 0.76) and confirming

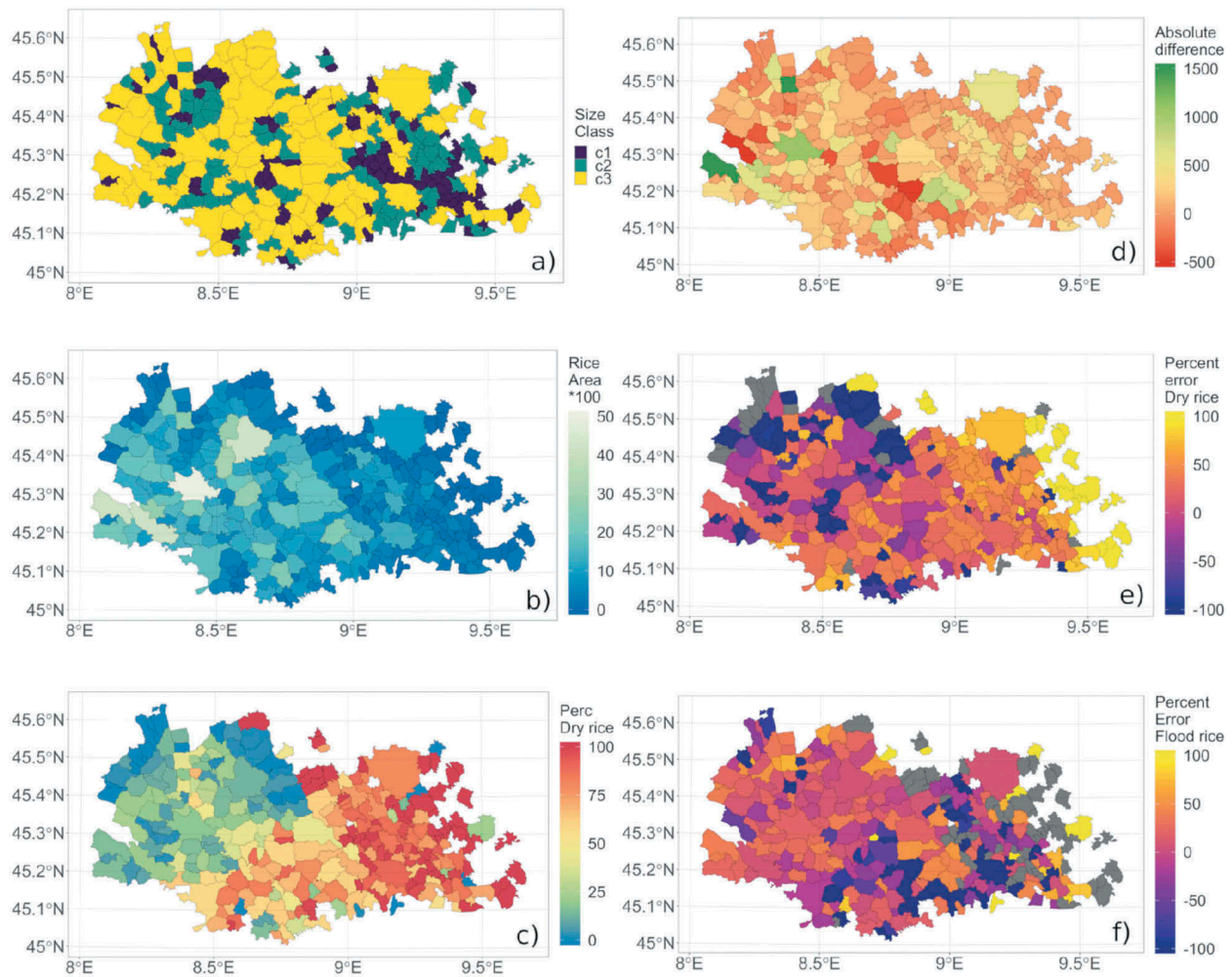


**Figure 8.** (a) Municipality size category as classified based on the histogram of the size distribution; (b) rice area aggregated at the municipality scale in [100 \* ha]; (c) percentage of dry rice within each municipality as estimated by ENR reference data; (d) absolute difference between ENR and EO estimated total rice area aggregated over the municipality; (e) and (f) percent error separated for the two classes *dry rice* and *flooded rice*. In the last two panels grey polygons show municipalities where either EO or ENR rice area is equal to 0.

robustness and exportability. The operational availability of Sentinel-1B data (from 2017) and Sentinel 2 A (from 2015) and B (from 2017) will further improve the frequency of observation and spatial resolution thus enhancing mapping accuracy.

Mapping flooding frequency was carried out by applying a RG algorithm, which exploits the low backscattering coefficient of water and built on S1A  $\sigma_{VV}^0$  multi-temporal images. Validation of flooded area maps was done by comparison with simultaneous dates of high-resolution SPOT5 (Take5) images showing good agreement for flooding maps which provides a picture of paddy fields at the date of data acquisition. By applying the RG algorithm, pixel-level (10 m) flooding mapping was performed with overall accuracy in the range 70–88% before the stage of canopy closure (first two dates available for validation: 5 May, 22 May 2015). On these early stages of rice growing, since vegetation cover is low, surface spectral signal is influenced also by the soil/water background; hence, the presence of water can be more easily detected. At

later stages, when greater and/or full vegetation canopy cover is reached, the spectral signal is influenced only by crop canopy conditions and characteristics; thus, the presence of water below the canopy cannot be detected. On the last date available for validation of flooding maps, an overall accuracy of 99% is reached but this high value is driven by the agreement of not flooded areas on both classified and reference datasets; however, given the full canopy closure at this stage, nothing can be inferred on the presence/absence of water below the canopy.

The comparison with official ENR statistics at the municipality scale is of great interest to prove that EO-based mapping could support the institutional task of providing official figures on rice cultivated areas by integrating farmer declarations; EO products could provide high-resolution spatial explicit crop information. Results show good agreement between EO estimates and ENR actual values of rice area at the municipality scale. We observed negligible influence of the municipality size on both the rice cultivated area (large

municipalities could have small rice cultivated areas and vice versa) and the accuracy of EO estimates. Generally, our approach leads to underestimate the actual rice, and larger per cent errors occur where rice cultivated surface over the municipality is less than 25 ha.

Recent changes in management of rice cultivations, which foresee the introduction of winter cover crops and the increase of dry seeding techniques, reduce mapping accuracy of the *dry rice* class although agreement coefficients at the municipality scale are satisfactory ( $r^2 = 0.71$  and MAE = 142.5 ha).

Maps in Figure 8(a, b) clearly show that dry seeding rice is mainly located in the eastern regions of the study area where the agricultural landscape is also more fragmented (small fields and different crops); in fact, panel d in the same figure clearly shows that total rice area is lower in these regions. On the contrary, flooded rice is practised in the western regions (towards the border with Piedmont). Looking at the distribution of the absolute difference and per cent errors between ENR and EO rice area aggregated at the municipality scale (Figure 8(d–f), larger discrepancies (green and red areas in Figure 8(d)) do not occur over larger municipalities since the total rice cultivated area is not related to the size of the administrative level. In the eastern regions, devoted to dry seeding rice, per cent error reaches higher values (~ 100%) although this apparently significant underestimation leads to less important absolute error (orange areas in Figure 8(d)) where the landscape is very fragmented and characterized by small fields cultivated with different crop species. Underestimation is confirmed also by scatterplots shown in Figure 7.

In general, performance indicators show that the accuracy of our results is satisfactory given the complexity of the agricultural land management and crop practices and the fact that mapping is carried out early in the season to better address water and crop management during the season. Comparable estimates are provided by official institution, such as ENR, but these databases are available after rice harvesting and therefore are of little utility for in-season management purposes.

## Conclusions

Spatially distributed products on rice seeding technique and flooding management are key information for regional planning and management of water resources. Early season rice mapping was carried out with Sentinel-1A and Landsat OLI images over northern Italy for the year 2015. A rule-based algorithm was built on synthetic features derived from multi-temporal series of both optical and SAR images. Rice mapping overall accuracy is 87.8% with commission and omission errors of 3.5% and 24.7%, respectively. We further discriminated between *dry* and *flooded rice* to provide information on rice seeding technique with  $r^2 > 0.70$

when compared to reference data at municipality scale. Finally, flooding maps were extracted with a RG algorithm with overall accuracy above 70%.

The rule-based algorithm developed in this work will be applied in the future to the archive of Landsat imagery for analysing changes in rice agronomic patterns (i. e. rice area and flooding timing) in the framework of a changing climate. Furthermore, the algorithm will be tested with Sentinel 2 data and enhanced accuracy is expected because of the increased spatial resolution and revisiting time.

## Acknowledgments

S5T5 images were acquired within the SPOT5 (Take5) experiment jointly conducted by CNES (Centre National d'Etudes Spatiales) and ESA (<https://spot-take5.org>). Cadastral polygons over Lombardy were provided the framework of the Space4Agri project (<http://space4agri.irea.cnr.it/it>). We acknowledge anonymous reviewers for their valuable comments.

## Disclosure statement

No potential conflict of interest was reported by the authors.

## Funding

This research was carried out within the ERMES FP7 project (<http://www.ermes-fp7space.eu>) funded by the European Union Seventh Framework Program (FP7/2007-2013) under Grant 606983

## ORCID

D. Stroppiana  <http://orcid.org/0000-0002-5619-4305>  
 Mirco Boschetti  <http://orcid.org/0000-0003-2156-4166>  
 G. Fontanelli  <http://orcid.org/0000-0002-3790-8288>  
 L. Busetto  <http://orcid.org/0000-0001-9634-6038>

## References

- Asilo, S., de Bie, K., Skidmore, A., Nelson, A., Barbieri, M., & Maunahan, A. (2014). Complementarity of two rice mapping approaches: Characterizing strata mapped by hypertemporal MODIS and rice paddy identification using multitemporal SAR. *Remote Sensing*, 6, 12789–12814. doi:10.3390/rs61212789
- Azar, R., Villa, P., Stroppiana, D., Crema, A., Boschetti, M., & Brivio, P.A. (2016). In-season mapping of crop type with optical and X-band SAR data: A classification tree approach using synoptic seasonal features. *Remote Sensing*, 7(19), 12859–12886.
- Bastarrica, A., Chuvieco, E., & Martinc, M.P. (2011). Mapping burned areas from Landsat TM/ETM+ data with a two-phase algorithm: Balancing omission and commission errors. *Remote Sensing of Environment*, 115(4), 1003–1012. doi:10.1016/j.rse.2010.12.005
- Bordogna, G., Kliment, T., Frigerio, L., Brivio, P.A., Crema, A., Stroppiana, D., ... Sterlacchini, S. (2016). Spatial data infrastructure integrating multisource heterogeneous

- geospatial data and time series: A study case in agriculture. *ISPRS International Journal of Geo-Information*, 5 (73). doi:10.3390/ijgi5050073
- Boschetti, M., Busetto, L., Manfron, G., Laborte, A., Asilo, S., Pazhanivelan, S., & Nelson, A. (2017). PhenoRice: A method for automatic extraction of spatio-temporal information on rice crops using satellite data time series. *Remote Sensing of Environment*, 194, 347–365. doi:10.1016/j.rse.2017.03.029
- Boschetti, M., Nutini, F., Manfron, G., Brivio, P.A., & Nelson, A. (2014). Comparative analysis of normalised difference spectral indices derived from MODIS for detecting surface water in flooded rice cropping systems. *PLoS one*, 9(2), e88741. doi:10.1371/journal.pone.0088741
- Boschetti, M., Stroppiana, D., Brivio, P.A., & Bocchi, S. (2009). Multi-year monitoring of rice crop phenology through time series analysis of MODIS images. *International Journal of Remote Sensing*, 30, 4643–4662. doi:10.1080/01431160802632249
- Bouvet, A., & Le Toan, T. (2011). Use of ENVISAT/ASAR wide-swath data for timely rice fields mapping in the mekong river delta. *Remote Sensing of the Environment*, 115, 1090–1101. doi:10.1016/j.rse.2010.12.014
- Brown, J.C., Kastens, J.H., Coutinho, A.C., Victoria, D.D. C., & Bishop, C.R. (2013). Classifying multiyear agricultural land use data from Mato Grosso using time-series MODIS vegetation index data. *Remote Sensing of the Environment*, 130, 39–50. doi:10.1016/j.rse.2012.11.009
- Busetto, L., Casteleyn, S., Granell, C., Pepe, M., Crema, A., Barbieri, M., ... Boschetti, M. (2017). Downstream services for rice crop monitoring in Europe: From regional to local scale. *IEEE Journal of Selected Topics in Applied Earth Observations and Remote Sensing*, 10(12), 5423–5441. doi:10.1109/JSTARS.2017.2679159
- Campos-Taberner, M., García-Haro, F.J., Camps-Valls, G., Grau-Muedra, G., Nutini, F., Busetto, L., ... Boschetti, M. (2017). Exploitation of SAR and optical sentinel data to detect rice crop and estimate seasonal dynamics of leaf area index. *Remote Sensing*, 9(3), 248. doi:10.3390/rs9030248
- Cesari de Maria, S., Rienzi, M., Facchi, A., Chiaradia, E.A., Romani, M., & Gandolfi, C. (2016). Water balance implications of switching from continuous submergence to flush irrigation in a rice-growing district. *Agricultural Water Management*, 171, 108–119. doi:10.1016/j.agwat.2016.03.018
- Chakraborty, A., Sachdeva, K., & Joshi, P.K. (2016). Mapping long-term land use and land cover change in the central Himalayan region using a tree-based ensemble classification approach. *Applied Geography*, 74, 136–150. doi:10.1016/j.apgeog.2016.07.008
- Choudhury, I., & Chakraborty, M. (2006). SAR signature investigation of rice crop using Radarsat data. *International Journal of Remote Sensing*, 27, 519–534. doi:10.1080/01431160500239172
- De Grandi, G.F., Leysen, M., Lee, J.S., & Schuler, D. 1997. “Radar reflectivity estimation using multiplicative SAR scenes of the same target: Technique and applications.” *Proceedings of International Geoscience and Remote Sensing Symposium (IGARSS)*, Singapore, 03–08 August, vol. 2, pp. 1047–1050.
- Dong, J., & Xiao, X. (2016). Evolution of regional to global paddy rice mapping methods: A review. *ISPRS Journal of Photogrammetry and Remote Sensing*, 119, 214–227. doi:10.1016/j.isprsjprs.2016.05.010
- ENR, (2016). XLVIII Relazione Annuale, Anno 2015, Il Riscoltore (report), electronically archived, [http://www.enterisi.it/upload/enterisi/bilanci/Relaz.Risi2015DEF\\_15916\\_312.pdf](http://www.enterisi.it/upload/enterisi/bilanci/Relaz.Risi2015DEF_15916_312.pdf).
- Fang, H.L., Wu, B.F., Liu, H.Y., & Huang, X. (1998). Using NOAA AVHRR and Landsat TM to estimate rice area year-by-year. *International Journal of Remote Sensing*, 19, 521–525. doi:10.1080/014311698216134
- Fontanelli, G., Crema, A., Azar, R., Stroppiana, D., Villa, P., & Boschetti, M. 2014. “Agricultural crop mapping using optical and SAR multi-temporal seasonal data: A case study in Lombardy region, Italy.” In *Proceedings of the IEEE International Geoscience and Remote Sensing Symposium*, Quebec City, Canada, 13–18 July 2014, 1489–1492.
- Ghazaryan, G., Dubovyk, O., Löw, F., Lavreniuk, M., Kolotii, A., Schellberg, J., & Kussul, N. (2018). A rule-based approach for crop identification using multi-temporal and multi-sensor phenological metrics. *European Journal of Remote Sensing*, 51(1), 511–524. doi:10.1080/22797254.2018.1455540
- Gumma, M.K., Thenkabail, P.S., Hideto, F., Nelson, A., Dheeravath, V., Busia, D., & Rala, A. (2011). A Mapping irrigated areas of Ghana using fusion of 30 m and 250 m resolution remote-sensing data. *Remote Sensing*, 3, 816–835. doi:10.3390/rs3040816
- Hao, P., Zhan, Y., Wang, L., Niu, Z., & Shakir, M. (2015). Feature selection of time series MODIS data for early crop classification using random forest: A case study in Kansas, USA. *Remote Sensing*, 7(5), 5347–5369. doi:10.3390/rs70505347
- Huete, A., Didan, K., Miura, T., Rodriguez, E.P., Gao, X., & Ferreira, L.G. (2002). Overview of the radiometric and biophysical performance of the MODIS vegetation indices. *Remote Sensing of Environment*, 83(1–2), 195–213. doi:10.1016/S0034-4257(02)00096-2
- Kamthonkiat, D., Honda, K., Turrall, H., Tripathi, N.K., & Wuwongse, V. (2005). Discrimination of irrigated and rainfed rice in a tropical agricultural system using SPOT VEGETATION NDVI and rainfall data. *International Journal of Remote Sensing*, 26, 2527–2547. doi:10.1080/01431160500104335
- Kirches, G., Brockmann, C., Boettcher, M., Peters, M., Bontemps, S., Lamarche, C., ... Defourny, P. 2014. “Land Cover CCI Product User Guide: Version 2.”
- Kuenzer, C., & Knauer, K. (2013). Remote sensing of rice crop areas. *International Journal of Remote Sensing*, 34 (6), 2101–2139. doi:10.1080/01431161.2012.738946
- Monaco, F., Sali, G., Hassen, M.B., Facchi, A., Romani, M., & Valè, G. (2016). Water management options for rice cultivation in a temperate area: A multi-objective model to explore economic and water saving results. *Water*, 8, 336. doi:10.3390/w8080336
- Mosleh, M.K., Hassan, Q.K., & Chowdhury, E.H. (2015). Application of remote sensors in mapping rice area and forecasting its production: A review. *Sensors*, 15, 769–791. (Basel). doi:10.3390/s150100769
- Nelson, A., Setiyono, T., Rala, A., Quicho, E., Raviz, J., Abonete, P., ... Ninh, N.H. et al. (2014). Towards an operational SAR-based rice monitoring system in Asia: Examples from 13 demonstration sites across Asia in the riice project. *Remote Sensing*, 6, 10773–10812. doi:10.3390/rs61110773
- Nguyen, D., Gruber, B.A., & Wagner, W. (2016). Mapping rice extent and cropping scheme in the Mekong delta using sentinel-1A data. *Remote Sensing Letters*, 7(12), 1209–1218. doi:10.1080/2150704X.2016.1225172
- Oguro, Y., Suga, Y., Takeuchi, S., Ogawa, M., Konishi, T., & Tsuchiya, K. (2001). Comparison of SAR and optical sensor data for monitoring of rice plant around Hiroshima. *Advances in Space Research*, 28(1), 195–200, ISSN 0273-1177, doi:10.1016/S0273-1177(01)00345-3.

- Pagani, V., Guarnieri, T., Busetto, L., Ranghetti, L., Boschetti, M., Movedi, E., ... Confalonieri, R. (2019). A high-resolution, integrated system for rice yield forecasting at district level. *Agricultural Systems*, 168, 181–190. doi:10.1016/j.agry.2018.05.007
- Ranghetti, L., Busetto, L., Crema, A., Fasola, M., Cardarelli, E., & Boschetti, M. (2016). Testing estimation of water surface in Italian rice district from MODIS satellite data. *International Journal of Applied Earth Observation and Geoinformation*, 52, 284–295. ISSN: 0303-2434. doi:10.1016/j.jag.2016.06.018.
- Ranghetti, L., Cardarelli, E., Boschetti, M., Busetto, L., & Fasola, M., (2018). *Assessment Ofwater Management Changes in The Italian Rice Paddies from 2000 to 2016 Using Satellite Data: a Contribution to Agro-ecological Studies, Remote Sensing*, 10, 416; doi: 10.3390/rs10030416.
- Shao, Y., Fan, X.T., Liu, H., Xiao, J.H., Ross, S., Brisco, B., ... Staples, G. (2001). Rice monitoring and production estimation using multitemporal RADARSAT. *Remote Sensing of Environment*, 76, 310–325. doi:10.1016/S0034-4257(00)00212-1
- Shi, J.J., Huang, J.F., & Zhang, F. (2013). Multi-year monitoring of paddy rice planting, area in Northeast China using MODIS time series data. *Journal of Zhejiang University*, 14(10), 934–946. doi:10.1631/jzus.B1200352
- Stroppiana, D., Bordogna, G., Carrara, P., Boschetti, M., Boschetti, L., & Brivio, P.A. (2012). A method for extracting burned areas from Landsat TM/ETM+ images by soft aggregation of multiple Spectral Indices and a region growing algorithm. *ISPRS Journal of Photogrammetry and Remote Sensing*, 69, 88–102. doi:10.1016/j.isprsjprs.2012.03.001
- Sun, H.S., Huang, J.F., Huete, A.R., Peng, D.L., & Zhang, F. (2009). Mapping paddy rice with multi-date moderate-resolution imaging spectroradiometer (MODIS) data in China. *Journal of Zhejiang University*, 10, 1509–1522. doi:10.1631/jzus.A0820536
- Torbick, N., Salas, W., Xiao, X., Ingraham, P., Fearon, M. G., Biradar, C., ... Zhao, Y. (2011). Integrating SAR and optical imagery for regional mapping of paddy rice attributes in the Poyang Lake Watershed, China. *Journal Canadian Journal of Remote Sensing*, 37, 17–26. doi:10.5589/m11-020
- Twele, A., Cao, W., Plank, S., & Martinis, S. (2016). Sentinel-1-based flood mapping: A fully automated processing chain. *International Journal of Remote Sensing*, 37(13), 2990–3004. doi:10.1080/01431161.2016.1192304
- Vaudour, E., Noirot-Cosson, P.E., & Membrive, O. (2015). Early-season mapping of crops and cultural operations using very high spatial resolution Pléiades images. *International Journal of Applied Earth Observation and Geoinformation*, 42, 128–141. ISSN 0303-2434. doi:10.1016/j.jag.2015.06.003.
- Villa, P., Stroppiana, D., Fontanelli, G., Azar, R., & Brivio, P.A. (2015). In-Season mapping of crop type with optical and X-Band SAR data: A classification tree approach using synoptic seasonal features. *Remote Sensing*, 7(10), 12859–12886. doi:10.3390/rs71012859
- Wittwer, R.A., Dorn, B., Jossi, W., & van der Heijden, M.G. A. (2017). Cover crops support ecological intensification of arable cropping systems. *Scientific Reports*, 7, 41911. doi:10.1038/srep41911
- Xiao, X., Boles, S., Froelking, S., Salas, W., Moore, B.I.I.I., Li, C., ... Zhao, R. (2002). Landscape scale characterization of cropland in China using Vegetation and Landsat TM images. *International Journal of Remote Sensing*, 23, 3579–3594. doi:10.1080/01431160110106069
- Yu, L., Wang, J., Clinton, N., Xin, Q., Zhong, L., Chen, Y., & Gong, P. (2013). FROM-GC: 30 m global cropland extent derived through multisource data integration. *International Journal of Digital Earth*, 6, 521–533. doi:10.1080/17538947.2013.822574
- Zhong, L., Hu, L., Gong, L.Y.P., & Biging, G.S. (2016). Automated mapping of soybean and corn using phenology. *ISPRS Journal of Photogrammetry and Remote Sensing*, 119, 151–164. ISSN 0924-2716. doi:10.1016/j.isprsjprs.2016.05.014.